J Mater Sci (2010) 45:259–267
DOI 10.1007/s10853-009-3928-3

A novel rock-like nanoarchitecture of $YVO_4:Eu^{3+}$ phosphor: selective synthesis, characterization, and luminescence behavior

S. Ray · A. Banerjee · P. Pramanik

Received: 22 June 2009 / Accepted: 24 September 2009 / Published online: 14 October 2009

Abstract A facile, surfactant-mediated strategy involving 'oriented attachment' assisted self-assembly of rice-like and grape-like nanostructures resulted into a novel encapsulated rock-like luminescent $YVO_4:Eu^{3+}$ nanoarchitecture in aqueous medium. It is shown that a characteristic crystallization behavior of $YVO_4:Eu^{3+}$ leads to the growth of a rice-like shape in a template-free reaction system. In presence of a surfactant, these rice-like structures in the vicinity of the micellar head groups self-assemble to form nanograpes and ultimately produce rock-like nanostructures upon prolonged autoclaving. The rock-like nanocrystalline phosphors, having an average area of 2798 nm^2, are composed of an inner nucleus and a surrounding shell-like cover, as evidenced from the transmission electron microscopy images. Finally, the room temperature photoluminescence spectra demonstrate that the morphology of the nanophosphors has immense influence on their chromaticity.

Introduction

Phosphors are of primary importance in science and technology due to their varied application in lighting devices, biological labeling motivates, and display units [1]. Size, shape, and dimensionality strongly affect the properties of nanostructured materials [2]. Indeed, dimensionality-modulated materials are highly desirable for advanced nanoscale electronic and optoelectronic applications [3]. Therefore, it is not surprising that the architectural control of nanocrystalline phosphors with well-defined shapes is a challenging and potentially rewarding goal in material chemistry. As these potential applications are very much in the design phase, further fundamental research in this field is essential [4].

In case of rare-earth ion doped phosphors, the electronic wave functions of rare-earths 4*f*–4*f* transitions are strongly localized, and they are not affected by quantum confinement effect. However, the spontaneous emission probability of optical transitions (luminescence lifetime) from rare-earth ions doped in nanoparticles may change with particle size, shape, and surrounding medium [5–7]. The luminescence lifetime may change owing to modifications in the (i) photon emission probability and/or (ii) phonon emission probability. The phonon density-of-states of the host material can be significantly modified according to the size and shape of the nanoparticles. Consequently, these changes of nonradiative relaxation probabilities (multiphonon emission) affect the luminescence lifetime as well as the quantum efficiency of the phosphor. Research in the field of shape-modulated synthesis of rare-earth-doped phosphors, therefore, is of scientific interest, as well as practical utility [8].

One family of host materials that has received a great deal of attention in the context of morphology-controlled fabrication of rare-earth-doped optical nanomaterials is the Orthovanadate of the Group 14 elements. The high luminescence quantum efficiency, the inherent stability, and availability of facile preparative routes for Group 14 Orthovanadates make these compounds extremely useful matrix materials in phosphors. As a consequence of the unique electronic structure and the numerous well-defined transition modes involving 4*f* shell of their ions, rare-earth ions entrapped in orthovanadate matrix constitute an important domain of the lanthanide-based nanostructure

S. Ray (✉) · A. Banerjee · P. Pramanik
Department of Chemistry, Indian Institute of Technology, Kharagpur, India
e-mail: sudeshnaiit@gmail.com

families [9]. In particular, YVO_4 has found application is several scientific and technological fields, such as the fabrication of efficient high-power polarizing prisms similar to Glan-Taylor prisms, use of Eu^{3+}-doped YVO_4 as a red phosphor in color televisions, CRTs and other display units [10], and fabrication of active laser materials such as Nd:YVO_4 for application in diode-pumped solid state lasers [11]. Notably, the product quality and performance of these devices are completely dependent upon the phosphors used. The excellent thermal stability, inherent sturdiness, and other physio-mechanical properties of YVO_4 make it a versatile and promising source for fabrication of several optical devices, under various conditions of usage.

Up to now, there has been no dearth of synthetic strategies employed to control the morphological development of nanocrystalline materials. Among the various methods employed for the synthesis of YVO_4 nanoparticles, colloidal routes [12, 13], solution combustion process [14], hydrolyzed colloid reaction [15], urea precipitation [16], and microemulsion-mediated synthesis [17] are important. Zhang et al. [18] have synthesized nanocrystalline YVO_4:Eu with the help of polyacrylamide gel method. By tuning the reaction conditions, such as yttrium-to-vanadium ratio, pH value, reaction temperature, time, and by use of organic molecules additives, Wu et al. [19] have tailored the size and shape of YVO_4 crystallites. Wu et al. [20] have also carried out template-mediated synthesis and study of different morphologies of YVO_4:Eu, along with spectroscopic investigation of the synthesized materials. There have been reports of other methods used for synthesis of Eu^{3+}-doped YVO_4 in different nanostructured variations, such as nanorods and microtubes [21]. Synthesis of different morphological varieties of rare-earth-doped YVO_4 nanoparticles has also been reported [22]. Till now, however, the rock-like morphology of YVO_4 nanoparticle has never been reported.

Herein, we report the formation of rice-like, grape-like, and rock-like morphological varieties of nanocrystalline YVO_4:Eu^{3+} phosphors. A hydrothermal synthesis in absence of any additives produced rice-like nanostructures. In presence of a cationic surfactant, Cetyl trimethyl ammonium bromide (CTAB), 'oriented attachment' assisted self-assembly of rice-like-doped YVO_4 nanocrystals resulted into grape-like YVO_4:Eu^{3+}. Finally, after prolonged autoclaving, rock-like nanocrystalline materials were generated in the micellar medium. It is to be noted that in this study, we: (1) report a novel 'oriented attachment' assisted aqueous solution strategy for controllable self-assembly of the rice-like nanostructures generated in situ; the strategy is especially appealing because of the low costs and potential application in large-scale production, and it may open a new avenue for tunable self-assembly of nanostructure into unique nanostructured materials; (2) obtain a grape-like nanostructure by side-by-side 'oriented attachment' of the nanorice; (3) obtain the aforementioned rock-like nanostructures by 'oriented attachment' assisted side-by-side and end-to-end self-assembly of nanograpes. The rock-like nanoarchitecture is being reported for the first time in this communication. The effect of host morphology on the photoluminescence (PL) properties of the phosphors has subsequently been studied with reference to the three as-formed nanostructures.

Experimental

Preparation of rice-like nanocrystalline sample

In a typical synthesis, an equimolar mixture of yttrium nitrate [$Y(NO_3)_3$] and ammonium vanadate (NH_4VO_3) (2 mmol of each reagent) was dissolved in 40 mL distilled water along with stoichiometric amount of $Eu(NO_3)_3$. The pH of the resulting solution was adjusted to 9 by drop wise addition of NH_4OH, leading to copious precipitation. The mixture thus obtained was then transferred to a 100 mL Teflon-lined stainless steel autoclave. It was sealed and maintained at 150 °C for 4 h, after which it was cooled to room temperature. Finally, the precipitate was filtered, washed with doubly distilled water, and afterwards with ethanol. The products were then dried at 70 °C in air, annealed at 800 °C for 3 h, and cooled to room temperature to obtain the rice-like morphology of YVO_4:Eu^{3+} (Eu^{3+}:4 at. wt%).

Preparation of grape-like nanocrystalline sample

The preparation procedure and the reagent quantity remained same as it were in the preparation of rice-like sample, except that 1.8 mmol CTAB was dissolved in distilled water and added to the mixture along with stirring. After the solution turned transparent, it was transferred to a 100 mL Teflon-lined stainless steel autoclave. The autoclave was sealed and maintained at 150 °C for 4 h, and then cooled to room temperature. Succeeding steps were repeated to recover the product.

Preparation of rock-like nanocrystalline sample

The procedure adopted for synthesis of grape-like samples was followed, except for the duration of autoclaving, which was changed to 12 h for the preparation of YVO_4:Eu^{3+} rock-like nanocrystalline sample (as opposed to 4 h for grape-like nanocrystalline sample).

Amount of $Eu(NO_3)_3$ was changed to vary the concentration of the dopant ion Eu^{3+}. The following Eu^{3+} concentrations were explored: 0.5, 2, 4, and 6 at. wt% of Eu^{3+} with respect to Y^{3+}.

Instrumentation

The phase identification was carried out by powder X-ray diffraction (XRD) at room temperatures, using a Philips PW1710 X-ray diffractometer, equipped with a vertical goniometer, and CuKα radiation source of wavelength 1.54 Å. The observation of morphology and selective area electron diffraction (SAED) were carried out using transmission electron microscopy (TEM). Samples for TEM were deposited onto 300 mesh copper TEM grids coated with 50 nm carbon films. Nanocrystals dispersed in acetone were placed on the grid drop wise. The excess liquid was allowed to evaporate in air. The grids were examined in JEOL 2010 microscope with ultra-high resolution pole piece using a LaB_6 filament operated at 200 kV. The Fourier transform infrared (FTIR) study was performed using a Shimadzu DT-40 model 883 IR Spectrophotometer. PL of the sample was investigated on Perkin-Elmer Luminescence Spectrometer LS50B at room temperature.

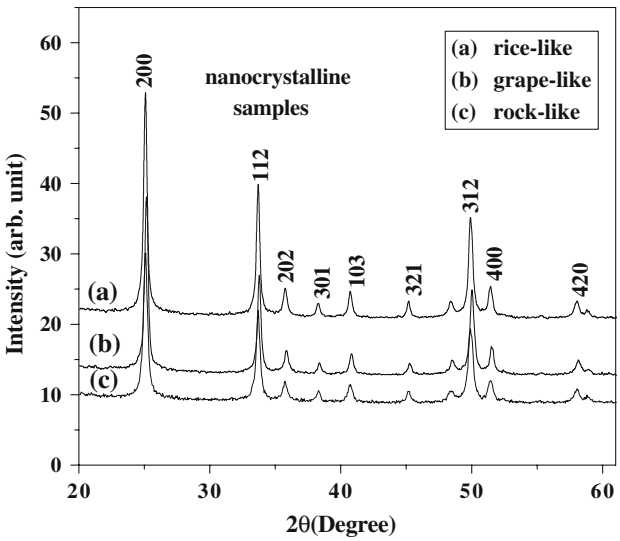

Fig. 1 XRD patterns of rice-like, grape-like, and rock-like nanocrystalline $YVO_4:Eu^{3+}$ samples

Results and discussion

X-ray diffraction

The XRD patterns of the three nanocrystalline samples are shown in Fig. 1. The nanocrystalline YVO_4 samples doped with 4 at. wt% Eu^{3+} were taken as reference, as they show the most intense PL emission spectra. The crystal structure obtained was of a pure tetragonal phase, which corresponds to the standard JCPDS (file no. 76-0341), for all the three different morphological varieties.

TEM and high-resolution transmission electron microscopy

Figure 2a–n represents the TEM and the high-resolution transmission electron microscopy (HRTEM) images of the samples. The morphological variations may be clearly seen from these images. A typical nanorice (Fig. 2a) shows a compressed equatorial diameter of 40 nm, while the elongated axial diameter is 160 nm, and is seen to have sharpened tips, resembling a grain of rice. Inset of Fig. 2a shows two typical rice-like nanocrystals. Figure 2b shows the corresponding frequency plot for the aspect ratios, which is obtained by measuring the same of many nanorices (obtained from a number of TEM images). The distribution (1.04) of the aspect ratios of the nanorices has been obtained from a Gaussian fit of the frequency plot. Figure 2c, d shows the HRTEM image and SAED pattern of a single nanorice. The HRTEM image clearly demonstrates the lattice fringes for the tetragonal phase of YVO_4 with good crystallinity. From the micrograph, we have determined the lattice spacing between different layers of rice-like nanocrystalline sample to be 2.22 Å, which corresponds to the (301) plane of tetragonal phase of YVO_4. SAED pattern of a single nanorice shows that they are polycrystalline in nature.

Figure 2e shows the grape-like morphology, which bears a crude resemblance to the nanorice prepared in absence of any surfactants, but is considerably less shriveled, with equatorial diameters of the order of 45 nm, and axial diameters of approximately 120 nm. Inset of Fig. 2e shows a grape-like nanocrystal. Figure 2f shows the frequency plot for the aspect ratios of the nanograpes. After Gaussian fit of the plot, the distribution in aspect ratio of nanograpes was found to be 0.33. Figure 2g, h shows the HRTEM image and SAED pattern of a single nanogrape. The HRTEM image shows the tetragonal phase of YVO_4 with good crystallinity, and from this image we can calculate the lattice spacing between different layers of the grape-like nanocrystalline sample to be 4.7 Å, which corresponds to the (101) plane of tetragonal phase YVO_4. As with the nanorice, SAED pattern of a single nanogrape shows that they are polycrystalline in nature.

The TEM images of the rock-like nanocrystalline samples are shown in Fig. 2i. This morphology shows some distinct features that make it worthy of special consideration. Inset of Fig. 2i shows a single rock-like nanocrystal. Figure 2j shows the frequency plot of the areas of the nanorocks (obtained with the help of 'Image J' image processing software). After Gaussian fit, the distribution in the area of the nanorock was found to be 1668 nm^2. The average area of these structures comes out to be 2798 nm^2. However, all these nanorocks show the presence of granular

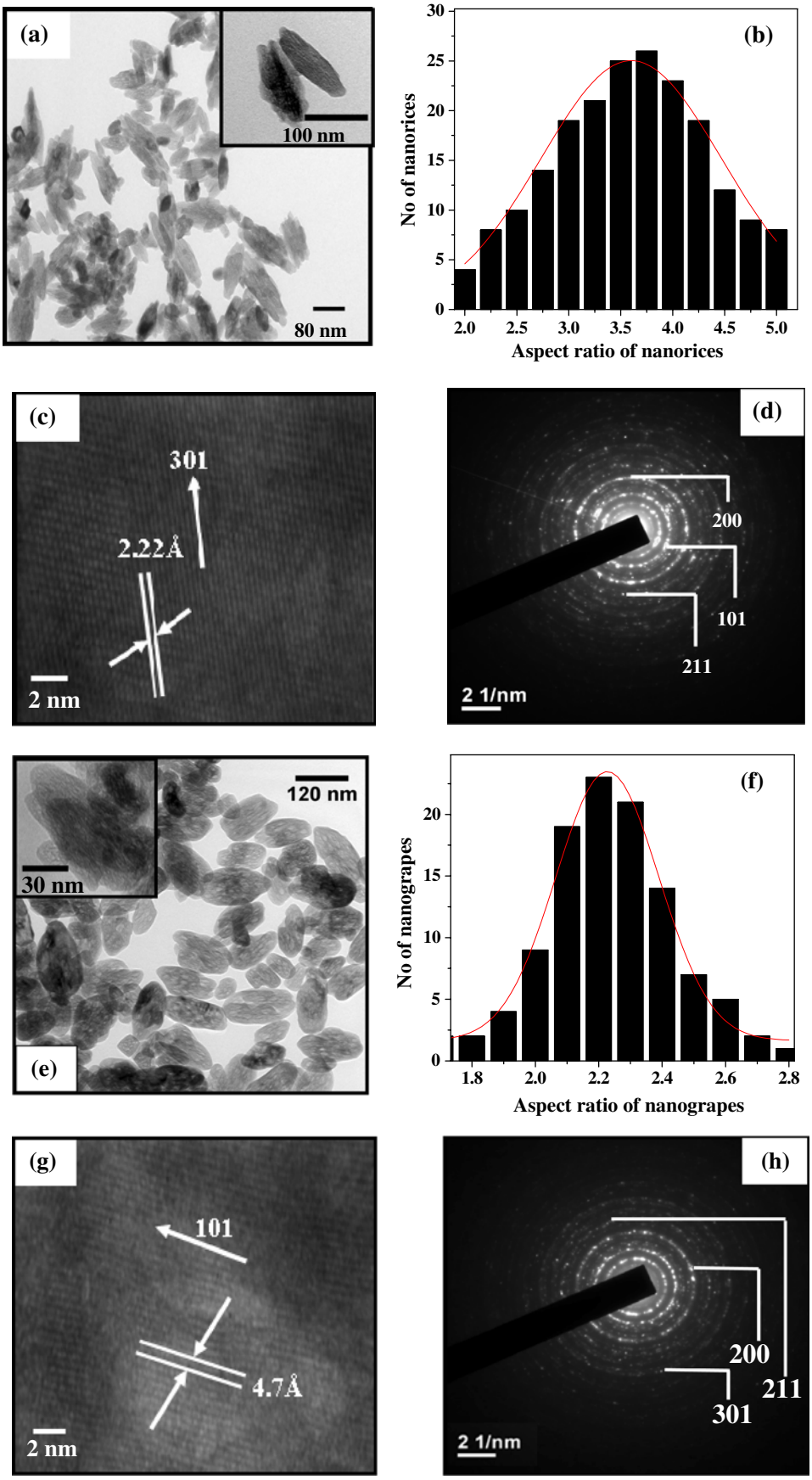

Fig. 2 **a** TEM micrograph of rice-like nanocrystalline samples (inset shows TEM micrograph of two rice-like nanocrystalline samples). **b** Frequency plot of $YVO_4:Eu^{3+}$ rice-like nanocrystalline samples. **c** HRTEM image of $YVO_4:Eu^{3+}$ rice-like nanocrystalline samples. **d** SAED pattern of $YVO_4:Eu^{3+}$ rice-like nanocrystalline samples. **e** TEM micrograph of grape-like nanocrystalline samples (inset shows TEM micrograph of two grape-like nanocrystalline samples). **f** Frequency plot of $YVO_4:Eu^{3+}$ grape-like nanocrystalline samples. **g** HRTEM image of $YVO_4:Eu^{3+}$ grape-like nanocrystalline samples. **h** SAED pattern of $YVO_4:Eu^{3+}$ grape-like nanocrystalline samples. **i** TEM micrograph of rock-like nanocrystalline samples (inset shows TEM micrograph of a single rock-like nanocrystalline sample). **j** Frequency plot of $YVO_4:Eu^{3+}$ rock-like nanocrystalline samples. **k** HRTEM image of $YVO_4:Eu^{3+}$ rock-like nanocrystalline samples. **l** SAED pattern of $YVO_4:Eu^{3+}$ rock-like nanocrystalline samples. **m** TEM images of grape-like nanocrystalline samples. *A* denotes the self-assembly of two grape-like nanocrystals. (↔) indicates the end-to-end and *B* (↻) denotes the side-to-side self-assembly of nanograpes. **n** TEM images of rock-like nanocrystals which results from the self-assembly of nanograpes

Fig. 2 continued

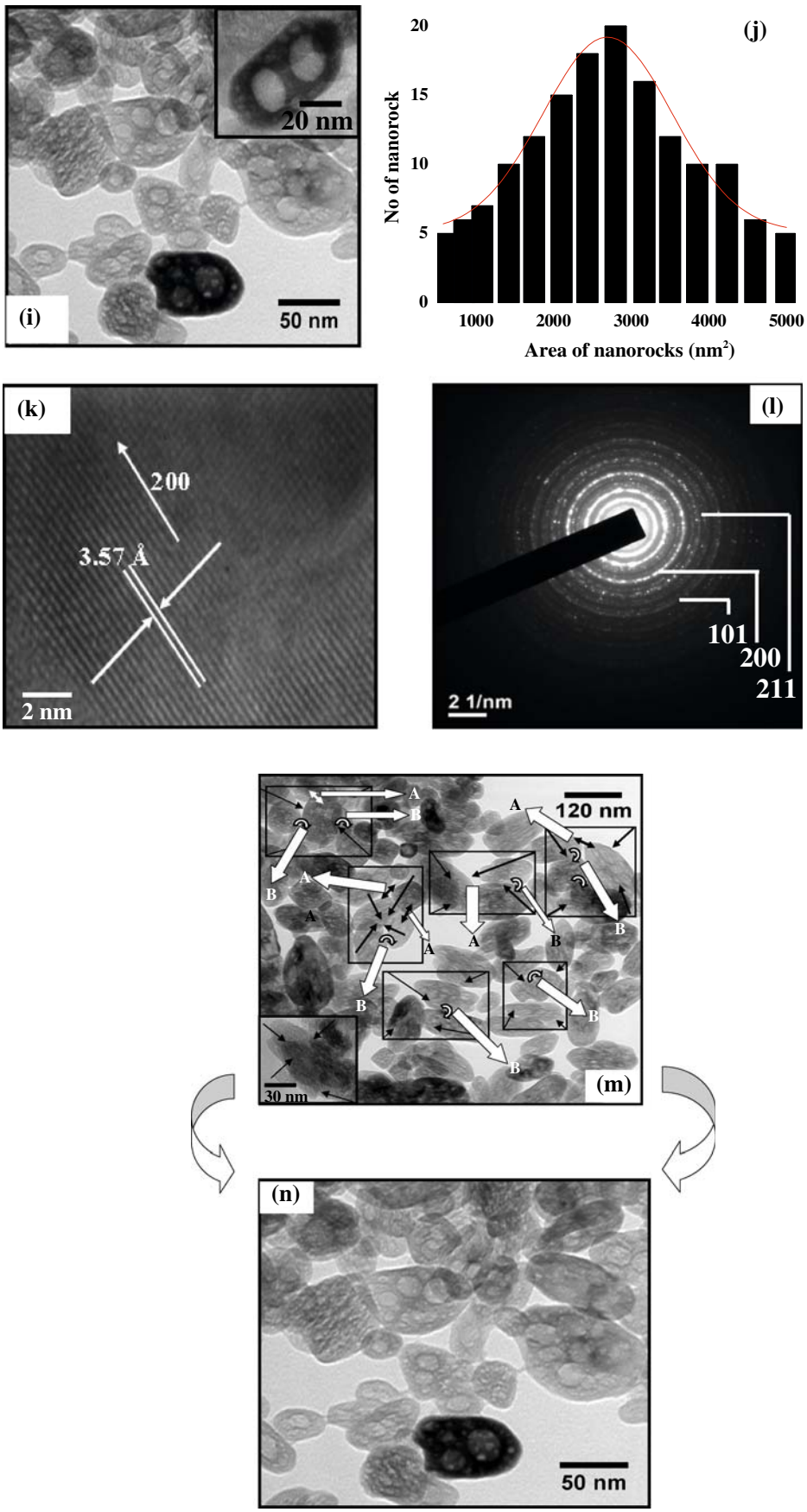

enclosures. The yolk-like cores show a size distribution, with diameters ranging from 5.2 to 15.7 nm. Figure 2k, l shows the HRTEM image and the SAED pattern of a single nanorock. From the HRTEM image of a single nanorock, the lattice spacing between different layers of nanorock is calculated to be 3.57 Å, corresponding to the (200) plane of the tetragonal phase of this material (YVO_4). HRTEM image of a single nanorock also reveals its highly crystalline nature. SAED pattern of a single nanorock shows that they are polycrystalline in nature.

Growth mechanism

A tentative formation mechanism may be suggested for the as-synthesized nanostructures, based on the reaction conditions under which they were generated. The TEM images shown in Fig. 2 reveal the effect of the cationic surfactant CTAB on the morphology of nanocrystalline-doped YVO_4. As shown in Fig. 2a, the rice-like nanocrystalline sample has an apically elongated structure, having a higher axial diameter than the equatorial one. The synthetic method adopted for the preparation of rice-like nanocrystalline sample does not operate in the presence of a catalyst, which can serve as the energetically favorable site for the selective adsorption of reactant molecules, as depicted in VLS mechanism. Nor does it involve the assistance of a template or a scaffold, which can guide the directional growth process [23]. Thus, it is suggested that the driving force for the anisotropic growth of YVO_4 nanorice is derived from the inherent crystal structure of YVO_4 crystals. Keeping all other parameters unchanged, when the reaction was carried out in presence of 1.8 mmol CTAB, the products formed were distinctly grape-like. This grape-like morphological variety has a lower aspect ratio than the rice-like structure. Thus, it can be concluded that the surfactant plays a crucial role during the growth of the grape-like nanostructures.

It is well known that when the concentration of the surfactant reaches a critical value (critical micellar concentration, CMC), the surfactant aggregates to form micelles. When 1.8 mmol of cationic surfactant CTAB was added into the mixture, the surfactants associate to form micellar aggregates ($CMC_{CTAB} = 4.8 \times 10^{-4}$ mol/L). These micelles bear positively charged headgroups, which electrostatically attract the VO_4^{3-} ions in the solution. This obviously leads to a preconcentration of the vanadate ions in the micellar vicinity. Now, Y^{3+} ions are attracted by vanadate ions. Hence, crystallization of YVO_4 nuclei occurs at a much faster rate at the surface of the micelles than in the bulk of the solution. In this way, many rice-like YVO_4 nuclei crystallize at the vicinity of the micellar headgroups. Under this reaction condition, the less shriveled, grape-like nanostructures are formed (Fig. 2e). This can be explained on the basis of 'oriented attachment' [24, 25] phenomenon, where rice-like YVO_4 nuclei 'stick' to each other by a side-by-side attachment [26]. Due to the preferentially equatorial self-assembly of rice-like nanostructures, nanograpes of lower aspect ratio are formed.

It is to be noted that the autoclaving was continued for 4 h during the synthesis of grape-like nanocrystals. When the autoclaving process was continued for 12 h, a unique morphological variety was obtained: the nanorock. This structure is clearly visible in Fig. 2i. The nanocrystalline rock-like sample also contains some granular enclosures, ranging in size from 2.5 to 5 nm. The effect of prolonged autoclaving is reflected in the rock-like nanostructures. The proposed growth mechanism is as follows: a number of normal micelle is present in the medium, and nanograpes, at the vicinity of headgroups of different micelle, start to self-assemble with each other. This self-assembly phenomenon may operate in an end-to-end as well as a side-by-side direction. The attachment of nanograpes present near the headgroups of a particular micelle and also around different micelle results in the formation of rock-like nanostructures. The YVO_4 nanorocks were synthesized in solution, and the formation process was via radial and axial 'oriented attachment' assisted self-assembly of nanograpes. To our knowledge, this unique formation process of the novel (rock-like) morphological variety has not been previously reported in the literature. The presence of yolk-like cores in nanorocks cannot be explained clearly and needs further investigation. The formation procedure of grape-like and rock-like morphological variety is schematically presented in Fig. 3.

FTIR spectra

The FTIR study was performed using a Shimadzu DT-40 model 883 IR Spectrophotometer. Figure 4 shows the FTIR spectra of the various morphologies of nanocrystalline Eu^{3+} (4 at. wt%)-doped YVO_4 samples. The different spectral features of Y(Eu)–VO_4, which emerge from the figure, may be summarized as follows: the strong IR band in the range of 780–920 cm^{-1} (obtained at $\sim$812 cm^{-1}) can be attributed to the (V–O) bond in VO_4^{3-}. The weak feature at 451 cm^{-1} corresponds to the Y(Eu)–O bonds [18, 20]. From Fig. 4, it can be seen that FTIR spectra are similar for the different morphological varieties. We know that FTIR spectrum can be taken as a 'molecular fingerprint' as it identifies different types of chemical bonds in a molecule [27]. The identical FTIR spectra of nanocrystalline YVO_4:Eu^{3+} samples with various morphologies indicate that the molecular structures as well as the chemical bonding are identical in all of them. Furthermore, although the samples have been prepared using reagents like CTAB, characteristic peaks of this reagent have not appeared in the FTIR spectra, indicating complete decomposition of the

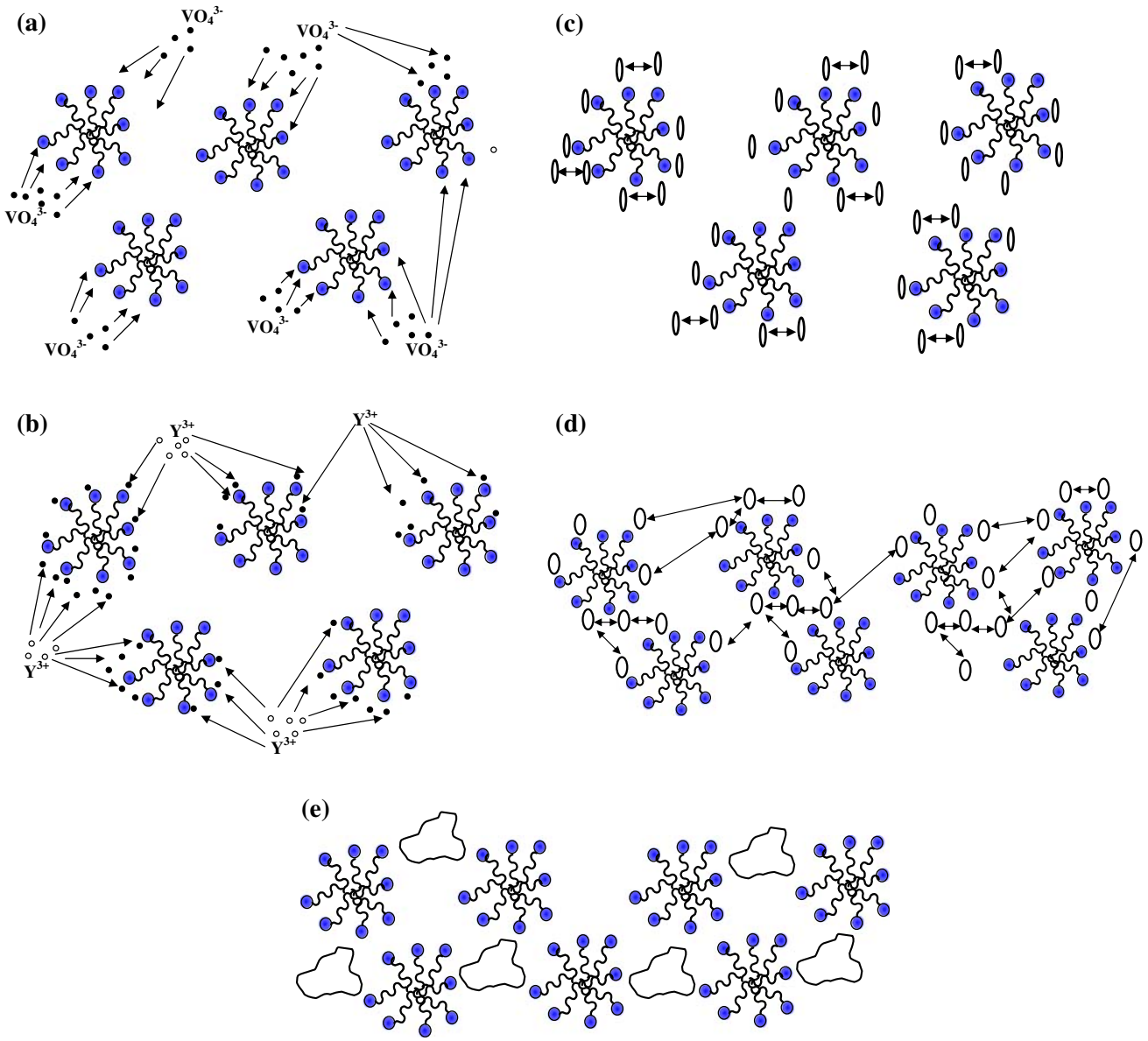

Fig. 3 Schematic representation of the formation of grape-like and rock-like nanocrystalline samples. **a** Preconcentration of VO_4^{3-} ions at the vicinity of positively charged headgroups of micelle. **b** Attachment of Y^{3+} ions by the VO_4^{3-} counter ions. **c** Appearance of rice-like YVO_4:Eu^{3+} nuclei at the vicinity of micellar headgroups. **d** Side-by-side attachment-assisted self-assembly of nanorice, grape-like nanostructure forms. **e** Axial and radial attachment-mediated self-assembly of nanograpes results in rock-like nanocrystalline samples

reagent after annealing the samples at 800 °C for 3 h. Thus, we get nanocrystalline-doped YVO_4 samples (rice-like, grape-like, and rock-like) in pure form.

Photoluminescence

Figure 5 shows the room temperature PL emission spectra of the as-synthesized nanorice, nanogrape, and nanorock of YVO_4:Eu^{3+} phosphors. Excitation of the VO_4^{3-} group at 280 nm generates the emission spectra, which consist of a series of emission lines between 580 and 750 nm, corresponding to transitions from the $^5D_0 \rightarrow {}^7F_J$ manifolds of Eu^{3+}. Among the transitions of Eu^{3+} originating from $^5D_0$ level, $^5D_0 \rightarrow {}^7F_1$ transition satisfies the magnetic dipole selection rules ($\Delta J = 0, \pm 1$ with $J = 0 \neq J' = 0$). The $^5D_0 \rightarrow {}^7F_2$ transition of Eu^{3+} is through forced electric dipole allowed type [28, 29]. The emission spectra of Eu^{3+} ion doped in these nanostructures are slightly broad as compared to the fine spectra of rare-earth ions. This broadening is attributed to the size distribution of nanorice,

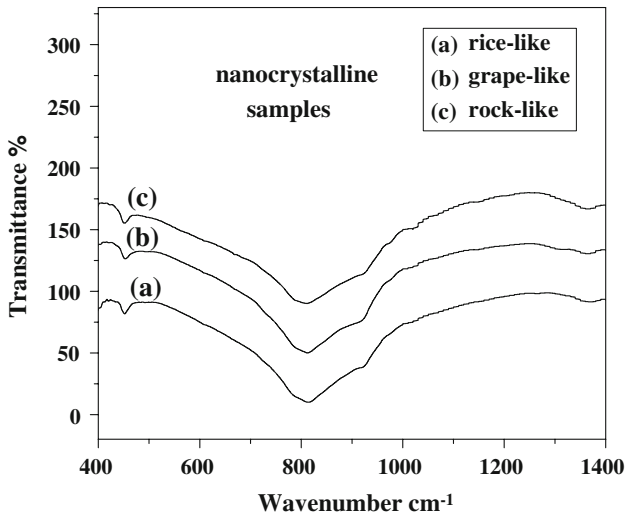

Fig. 4 FTIR spectra of nanocrystalline YVO_4:Eu^{3+} samples (rice-like, grape-like, and rock-like)

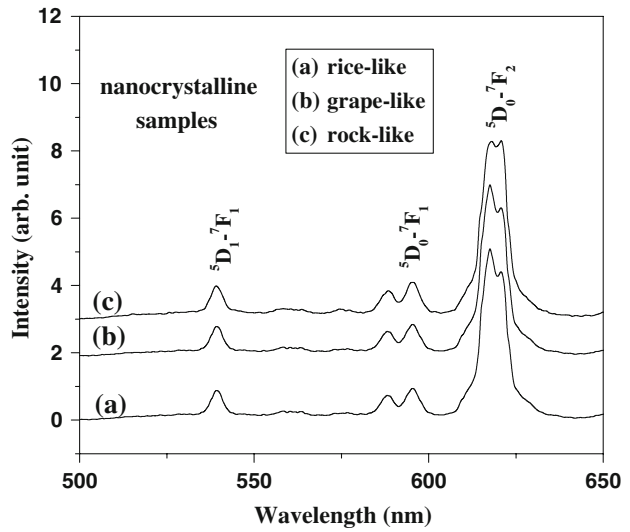

Fig. 5 PL emission spectra of nanocrystalline YVO_4:Eu^{3+} samples (rice-like, grape-like, and rock-like)

nanograpе, and nanorocks as shown in Fig. 2b, f, and j. Due to size distribution, the lattice parameter of the nanoparticles changes slightly, which causes the shifting of the energy level of Eu^{3+} ion [30]. These result in the broadening of the emission spectra of YVO_4:Eu^{3+} samples.

As reported in a previous work, for the bulk YVO_4:Eu^{3+}, the crystalline YVO_4 adopts the tetragonal structure, which is essentially composed of YO_8 dodecahedra (Y^{3+} has a point symmetry of D_{2d}, without an inversion center) and VO_4 tetrahedra (T_d) [31]. The Eu^{3+} ions occupy Y^{3+} sites in the doped YVO_4 samples. Thus, in the emission spectra of YVO_4:Eu^{3+}, the hypersensitive $^5D_0 \rightarrow {}^7F_2$ ($\Delta J = 2$) transition becomes the most prominent one. The intensity of the magnetic dipole transition ($^5D_0 \rightarrow {}^7F_1$)

Table 1 Values of red/orange emission intensities of Eu^{3+} in nanocrystalline YVO_4:Eu^{3+} phosphors with tunable morphologies

Morphology of the host	R/O			
	0.5 at. wt% Eu^{3+}	2 at. wt% Eu^{3+}	4 at. wt% Eu^{3+}	6 at. wt% Eu^{3+}
Rice-like	5.04	5.12	4.99	5.01
Grape-like	4.49	4.52	4.54	4.51
Rock-like	4.14	4.09	4.14	4.11

hardly changes with the crystal field strength around the Eu^{3+} ion, whereas the intensity of the hypersensitive electric dipole allowed transition ($^5D_0 \rightarrow {}^7F_2$) is highly sensitive to the local environment in the vicinity of the Eu^{3+} ions [32]. The PL intensity ratio of ($^5D_0 \rightarrow {}^7F_2$)/($^5D_0 \rightarrow {}^7F_1$) (red/orange) transitions gives a measure of the degree of distortion from the inversion symmetry of the local environment of Eu^{3+} ion in the matrix [33]. In fact, this ratio is generally called the asymmetry ratio. Therefore, the larger the value of the intensity ratio ($^5D_0 \rightarrow {}^7F_2$)/($^5D_0 \rightarrow {}^7F_1$), lower the symmetry around Eu^{3+} ion in the host. We observe that the intensity ratio (red/orange) varies with the change in the host morphology, but no appreciable changes are found with the variation in the concentration of the dopant ion. Therefore, the larger the value of intensity ratio ($^5D_0 \rightarrow {}^7F_2$)/($^5D_0 \rightarrow {}^7F_1$), lower the symmetry around Eu^{3+} ion in the host. Table 1 depicts the ($^5D_0 \rightarrow {}^7F_2$)/($^5D_0 \rightarrow {}^7F_1$) intensity ratio of Eu^{3+} ions (with four different concentrations) doped in nanocrystalline YVO_4 with different morphologies.

Conclusion

To summarize, we have demonstrated that the rock-like nanostructures of YVO_4:Eu^{3+} were obtained by side-by-side and end-to-end 'oriented attachment' mediated self-assembly of nanograpes in a micellar medium. The results presented in this article illuminate an interesting example of the effect of self-assembly of a particular nanostructure into another novel nanoarchitecture. The formation mechanism, which involves the attachment of rice-like nuclei of YVO_4 associated with headgroups of different micelle, is reported for the first time. This may surmized to be a model growth process, and is expected to be of a certain generality. By the suitable choice of source and synthetic parameters, it is reasonable to expect that this study could be extended to other self-assembled nanostructures. It has been observed from the PL studies on the as-prepared samples that the chromaticity of the phosphors varies with the change of the host morphology. These results indicate that the host morphology affects the local symmetry around

the dopant ions in the matrix, which ultimately affects the chromaticity of the phosphor.

References

1. Zeng JH, Li ZJ, Su J, Wang L, Yan R, Li Y (2006) Nanotechnology 17:3549
2. Murugan AV, Viswanath AK, Kakade B, Ravi V, Saaminathan V (2006) J Phys D Appl Phys 39:3974
3. Hu JT, Odom TW, Lieber CM (1999) Acc Chem Res 32:435
4. Ghosh P, Sadhu S, Patra A (2006) Phys Chem Chem Phys 8:3342
5. De G, Qin W, Zhang J, Zhang Y, Wang Y, Cao C, Cui Y (2006) J Lumin 258:119
6. Mehta A, Thundat T, Barnes MD, Chhabra V, Bhargava R, Bartko AP, Dickson RM (2003) Appl Opt 42:2132
7. Stouwdam JW, Van Veggel CJ (2002) Nano Lett 2:733
8. Ghosh P, Patra A (2008) J Nanosci Nanotech 8:3458
9. Bu W, Chen H, Hua Z, Liu Z, Huang W, Zhang L, Shi J (2004) Appl Phys Lett 85:4307
10. Levine AK, Pallilla FC (1964) Appl Phy Lett 5:118
11. Meng X, Zhu L, Zhang H, Wang C, Chow Y, Lu M (1999) J Cryst Growth 200:199
12. Riwotzki A, Haase M (1998) J Phys Chem B 102:10129
13. Huignard A, Buissette V, Laurent G, Gacoin T, Boilot J-P (2002) Chem Mater 14:2264
14. Kambaram SE, Patil KC (1995) J Alloys Compd 217:104
15. Erdei S, Schlecht R, Ravichandran D (1995) Displays 19:173
16. Newport A, Silver J, Vecht A (2000) J Electrochem Soc 147:3944
17. Sun LD, Zhang YX, Zhang J, Yan CH, Liao CS, Lu YQ (2002) Solid State Commun 124:35
18. Zhang H, Fu X, Niu S, Sun G, Xin Q (2004) J Solid State Chem 177:2649
19. Wu H, Xu H, Su Q, Chen T, Wu M (2003) J Mater Chem 13:1223
20. Wu X, Tao Y, Song C, Mao C, Dong L, Zhu J (2006) J Phys Chem B 110:15791
21. Wu X, Tao Y, Mao C, Liu D, Mao Y (2006) J Cryst Growth 290:207
22. Ray S, Banerjee A, Pramanik P (2009) Mater Sci Eng B 156:10
23. Wang X, Li Y (2002) Angew Chem Int Ed 41:4790
24. Cho K-S, Talapin DV, Gaschler W, Murray CB (2005) J Am Chem Soc 127:7140
25. Yu H, Joo J, Park H, Baik S-I, Kim YW, Kim SC, Hyeon T (2005) J Am Chem Soc 127:5662
26. Deng Z, Chen D, Tang F, Meng X, Ren J, Zhang J (2007) J Phys Chem C 111:5325
27. Silverstein RM, Webster FX, Kiemle D (2005) Spectrometric identification of organic compounds. Wiley, New York
28. Judd BR (1962) Phys Rev 127:750
29. Ofelt GS (1962) J Chem Phys 37:511
30. Manjo'n FJ, Jandl S, Riou G, Ferrand B, Syassen K (2004) Phys Rev B 69:165121
31. Yu M, Lin J, Wang Z, Fu J, Wang S, Zhang HJ, Hun Y (2002) Chem Mater 14:2224
32. Yu M, Lin J, Fang J (2005) J Chem Mater 17:1783
33. Su Q, Lin J, Li B (1995) J Alloys Compd 225:120